Structure and Energetics of $Fe_2(CO)_8$ Singlet and Triplet Electronic States

Luca Bertini,[†] Maurizio Bruschi,[‡] Luca De Gioia,[†] and Piercarlo Fantucci*[,†]

Department of Biotechnology and Biosciences, Universitá degli Studi di Milano-Bicocca, Piazza della Scienza, 2, 20126 Milan, Italy, and Department of Environmental Sciences, Universitá degli Studi di Milano-Bicocca, Piazza della Scienza, 1, 20126 Milan, Italy

Received: July 9, 2007; In Final Form: September 4, 2007

The singlet and triplet state potential energy surfaces (PES) of $Fe_2(CO)_8$ are explored by means of density functional theory (DFT) techniques. The two PES have different global mimima: the dibriged C_{2v} isomer for the singlet and the unbridged D_{2d} isomer for the triplet. The sign of the energy gap between singlet and triplet global minima depends on the type of adopted DFT functional: hybrid functionals predict the triplet is more stable than the singlet, but the opposite applies to generalized gradient approximated (GGA) functionals. The analysis of the computed CO stretching frequencies demonstrates that the experimental data for the unbridged form is compatible also with the unbridged triplet D_{2d} isomer. Starting from these two facts, the electronic structure of unbridged D_{2d} $Fe_2(CO)_8$ is discussed herein. Single-point energy computations at the coupled-cluster single and double (CCSD) level favor the D_{2d} triplet state.

1. Introduction

Binuclear homoleptic transition metal carbonyls are fundamental systems in organometalic chemistry, and the study of their chemistry and photochemistry is crucial to predict the behavior of higher nuclearity systems. $Fe_2(CO)_8$ is an unsaturated diiron carbonyl complex for which an iron−iron double bond was proposed to fulfill the 18-electron rule, in agreement with the isolobal analogy with ethylene.[1] This complex is also relevant because it can be considered as the all-CO prototype on the diiron cluster contained in the Fe-only hydrogenase enzymes, and the disclosure of its stereo-electronic proterties could be important for the chemical design of biomimetic complexes with catalytic activity.[2]

$Fe_2(CO)_8$ is a transient binuclear carbonyl complex observed in 1971 by Poliakoff and Turner[3] through CO photolysis of $Fe_2(CO)_9$ in matrices at a low temperature:

$$Fe_2(CO)_9 \xrightarrow{h\nu} Fe_2(CO)_8 + CO$$

The photolysis produces two isomers of $Fe_2(CO)_8$, the CO-bridged one and the unbridged one. In a second paper Fletcher, Poliakoff, and Turner[4] proposed the structure of the two isomers on the basis of their infrared (IR) spectra. Through the analysis of the CO stretching modes, the bridged isomer was found to be compatible with the C_{2v} dibridged structure. A second bridged structure of C_s symmetry was characterized through theoretical computation by Jacobsen and Ziegler.[7] These two structures may be considered as derivable from tribridged D_{3h} $Fe_2(CO)_9$ through dissociation of one μ-CO ligand or one terminal CO ligand, respectively (see Chart 1):

The D_{2h} symmetry has been assigned to the unbridged form on the basis of IR spectra[3] (see Chart 2), and it is consistent with the theoretical finding of Hoffmann[1] and Poliakoff et al.[3] In addition, Fletcher et al.[4] showed that the bridged $Fe_2(CO)_8$ is the major product of $Fe_2(CO)_9$ photolysis. However, through deposition of mass-selected cluster experiments, Fedrigo et al.[5] showed that the major product of the reaction between Fe_2^+ and CO is the unbridged $Fe_2(CO)_8$. The authors confirmed this result through the analysis of the IR spectra of the products, showing that the unbridged isomer is the major product, which is stable up to 50 K.

Further experimental work on this system dealt with the measurement of the CO dissociation energy of $Fe_2(CO)_x^+$ ($x =$

CHART 1

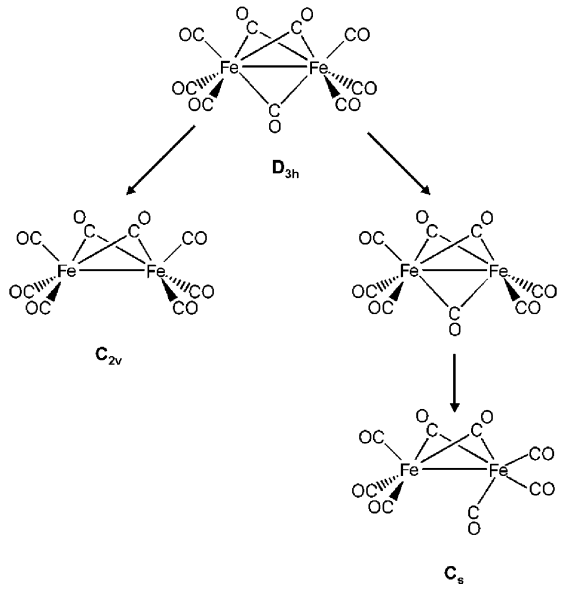

CHART 2

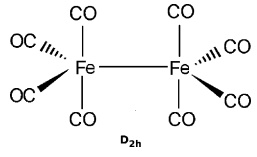

* To whom correspondence should be addressed. E-mail: piercarlo.fantucci@unimib.it.
† Department of Biotechnology and Biosciences.
‡ Department of Environmental Sciences.

10.1021/jp075343z CCC: $37.00
Published on Web 11/08/2007

1−9) cations through mass spectrometry measurement.[6] In particular, the energies determined for the reactions

$$Fe_2(CO)_9^+ \rightarrow Fe_2(CO)_8^+ + CO$$

$$Fe_2(CO)_8^+ \rightarrow Fe_2(CO)_7^+ + CO$$

are equal to 24.9 ± 2.5 and 7.6 ± 1.8 kcal·mol^{-1}, respectively.

$Fe_2(CO)_8$ has been the object of several theoretical papers. The first paper by Jacobsen and Ziegler[7] is an example of extensive density functional theory (DFT) study, showing that the dibridged C_s structure is the global minimum of the $Fe_2(CO)_8$ potential energy surface (PES). The D_{2h} unbridged form was found higher in energy in comparison to the C_s form. Through a trans-bent distortion of two axial CO ligands, the semibridged C_{2h} isomer was proposed as the unbridged form. Finally, the bridged-unbridged isomerization reaction path was proposed. In the second study by Barckholtz and Burstem,[8] an estimate of the energy for $Fe_2(CO)_9 \rightarrow Fe_2(CO)_8 + CO$ dissociation equal to 32.3 kcal·mol^{-1} was proposed on the basis of DFT calculations, in reasonable agreement with the experimental value of 28 kcal·mol^{-1}.[9,10] Xie et al.[11] presented a detailed investigation of the ground state PES of $Fe_2(CO)_8$ at DFT level, in the framework of a more comprehensive study on $Fe_2(CO)_x$ ($x = 6-9$) complexes. The dibridged C_{2v} structure was found to be the lowest in energy. The latest theoretical study was carried out in our laboratory[12] and dealt with the time-dependent DFT (TDDFT) modeling of the $Fe_2(CO)_9$ CO photolysis. We found that the first triplet and the second singlet excited PES have dissociative character with the formation of the $Fe_2(CO)_8$ bridged isomer. Finally, there is also a closely related theoretical paper on the $Fe_2(CO)_8^{2-}$ dianion,[13] in which the unbridged D_{2d} structure is found to be the ground state. The $Fe_2(CO)_8^-$ anion has also been experimentally investigated using gas-phase IR spectroscopy by Moore et al.[14]

Althought the singlet PES has been the subject of several theoretical papers, to the best of our knowledge triplet PES has never been investigated. Furthermore, in our previous work, we found that triplet $Fe_2(CO)_8$ is involved in the $Fe_2(CO)_9$ CO photolysis mechanism. Prompted by these consideration, in the present paper we are reporting a systematic investigation of the triplet PES of $Fe_2(CO)_8$ by means of DFT calculations. To compare our results with those of previous works, we also investigated the singlet PES. For all isomers, the vibrational spectra was calculated and compared with the experimental data.

We can anticipate that this analysis has shown that (i) the experimental IR spectra for the unbridged form is also compatible with a triplet D_{2d} structure and (ii) the DFT level of theory is not able to definitively assess the spin multiplicity of the ground state of $Fe_2(CO)_8$. On the basis of this evidence, we have considered the possibility of a high-spin ground state for $Fe_2(CO)_8$. This paper will be mainly focused on the discussion of this aspect.

2. Computational Details

In this paper computations were performed using pure gradient generalized approximation (GGA) BP86[15,16] and hybrid B3LYP[17,18] DFT functionals. Basis sets of triple-ζ plus polarization split valence quality (TZVP hereafter)[19] were adopted for all atoms in the complex. All computations were performed using the TURBOMOLE[20] suite of programs, which for BP86 functional are able to take advantage of the use of resolution of identity (RI) technique.[21,22] DFT grid size is set to standard *m*3 value. Geometry optimizations were carried out using 10^{-6} hartree convergence criterion on the total energy and 0.001 hartree·Å^{-1} for the gradient norm vector. Coupled-cluster single and double (CCSD) single-point energy computations were carried out with TZVP basis set using Gaussian03[23] suite of programs.

3. Results

The results of the exploration of singlet and triplet state PES are reported in Table 1. The optimized geometry parameters are reported in Figure 1 (singlets) and 2 (triplets). BP86 and B3LYP singlet and triplet state energies for the various structures under consideration are summarized in Figure 3.

As a general trend, B3LYP Fe−Fe and Fe−C distances are always longer than those of BP86, and the opposite is true for for C−O distances. The topologies of the B3LYP and BP86 singlet and triplet PES are similar, except in the case of some isomers for which the signature of stationary point is different.

The "DFT pairing problem", i.e., the ability of different density functionals to compute the properties of a molecular system in its high- and low-spin state is well documented[24−26] for transition metal complexes. In the present case, we have computed the adiabatic energy difference between singlet and triplet states of $Fe_2(CO)_8$

$$\Delta E_{\text{triplet}-\text{singlet}} = E_{\text{triplet}}(\mathbf{R}_{\text{eq}}^{\text{triplet}}) - E_{\text{singlet}}(\mathbf{R}_{\text{eq}}^{\text{singlet}}) \qquad (1)$$

where the vector $\mathbf{R}_{\text{eq}}$ collects the minimum geometry parameters. BP86 stabilizes the singlet states compared to triplet states in all cases but two. The value of this stabilization is generally uniform among the structures considered ($\Delta E_{\text{triplet}}^{\text{BP}_{86}} = 0.0097-0.0193$ hartree; average $\Delta E_{\text{triplet}-\text{singlet}}^{\text{BP}_{86}} = 0.0157$ hartree (9.86 kcal·mol^{-1})). B3LYP stabilizes the triplet states compared to singlet state in all the cases except one, and this stabilization is less uniform among the structure considered ($\Delta E_{\text{triplet}-\text{singlet}}^{\text{B}_3\text{LYP}} = 0.0012-0.0406$ hartree). These trends are in agreement with those found by Reiher et al.[44] for other transition metal complexes. The values of $\Delta E_{\text{triplet}-\text{singlet}}$ as a function of the DFT functional will be further analyzed in the discussion section.

3.1. Singlet PES. As the result of a systematic search, as many as seven stationary points were located on the singlet PES. Three of these isomers correspond to bridged forms, another three to unbridged forms and one to a semibridged form.

$^1C_{2v}$, ^1C_s, and $^1D_{2h}$ (2) Bridged Isomers. The $Fe_2(CO)_8$ PES has two genuine dibridged minima close in energy of C_s and C_{2v} symmetry, respectively. They can be obtained starting the geometry optimization from the tribridged D_{3h} $Fe_2(CO)_9$ without one terminal or without one bridged CO group, respectively. It is worth noting that ^1C_s and $^1C_{2v}$ forms can be related to the bridged and open forms of the [FeFe]-hydrogenase catalytic site.[28] In particular, the $^1C_{2v}$ form is structurally similar to the catalytic site in its active form, due to the presence of the semibridged CO ligand.[29]

At BP86 level, the ^1C_s form is the global minimum. The $^1C_{2v}$ structure at BP86 level is higher in energy with respect to the ^1C_s by only 0.0014 hartree (0.88 kcal·mol^{-1}). Also at the B3LYP level these two forms are almost isoenergetic, with the $^1C_{2v}$ slightly lower in energy. The optimized BP86 and B3LYP structures are quite similar, in particular in the case of the $^1C_{2v}$ form. For the ^1C_s form, the only significant difference between the two sets of geometry parameters is the Fe−C distance of the CO group bent toward the bridging region (2.851 Å BP86, 2.949 Å B3LYP).

The third dibridged stationary point is of D_{2h} symmetry (Figure 1, hereafter $^1D_{2h}(2)$) and lies higher in energy with

TABLE 1: Restricted $Fe_2(CO)_8$ Singlet and Triplet BP86/TZVP and B3LYP/TZVP PES

singlet	E_{BP86}[a]	δ_{BP86}[b]	E_{B3LYP}[a]	δ_{B3LYP}[b]	i_{BP86}[a]	i_{B3LYP}[c]	configuration	Fe−Fe_{BP86}[d]	Fe−Fe_{B3LYP}[d]
C_s	−3435.1768	0.0	−3433.9565	0.4	0i	0i	$50a'^2 30''^2$	2.482	2.517
C_{2v}	−3435.1754	0.9	−3433.9571	0.0	0i	0i	$29a_1^2 13a_2^2 24b_2^0$	2.454	2.455
C_{2h}	−3435.1666	6.4	−3433.9525	2.9	i6.7	i98.4	$28a_g^2 28b_u^2 29a_g^0$	2.587	2.628
D_{2h}	−3435.1544	14.1	−3433.9415	9.8	i62.2 i32.0 i12.2	i36.3 i34.2 i14.1	$19a_g^2 10b_{2u}^2 10b_{2g}^0$	2.549	2.544
$D_{2h}(2)$	−3435.1526	15.2	−3433.9371	12.6	i269.3	i301.1 i200.3	$22a_g^2 10b_{2u}^2 7b_{3g}^0$	2.529	2.564
$C_{2v}(2)$	−3435.1494	17.2	−3433.9443	8.0	i130.8	i119.1 i103.2	$37a_1^2 20b_2^0 20b_1^2$	2.454	2.513
$C_{2h}(2)$	−3435.1446	20.2	−3433.9276	18.5	i183.0 i88.6 i27.1	i248.3 i98.5 i34.3	$29a_u^2 13a_g^2 13b_g^0$	2.5301	2.559

triplet	E_{BP86}	δ_{BP86}	E_{B3LYP}	δ_{B3LYP}	i_{BP86}	i_{B3LYP}	configuration	Fe−Fe_{BP86}	Fe−Fe_{B3LYP}
D_{2d}	−3435.1727	0.0	−3433.9849	0.0	0i	0i	$37a_1^2 20b_2^1 20b_1^1$	2.492	2.543
C_{2v}	−3435.1592	12.6	−3433.9614	14.6	i151	i166.1	$29a_1^1 13a_2^2 24b_2^1$	2.606	2.644
C_s	−3435.1588	8.7	−3433.9694	9.7	i38.0	i26.9	$50a'^2 30a'' 31a''^1$	2.456	2.658
$D_{2h}(2)$	−3435.1543	11.5	−3433.8985	54.2	371.7i 346.7i 21.3i	i593.3 i504.3 i40.8	$18b_{1u}^2\ 10b_{2u}^1 7b_{3g}^1$	2.552	2.609
C_{2h}	−3435.1473	15.9	−3433.9583	16.7	i5.9	i27.1	$28a_g^2 28b_u^1 29a_g^1$	2.756	2.857
D_{2h}	−3435.1390	21.1	−3433.9551	18.7	44.6i 39.0i 34.3i 32.1i	i36.4 i31.4 i19.2	$19a_g^2 10b_{2u}^1 10b_{2g}^1$	2.910	2.948
D_{3d}	−3435.1349	23.7	−3433.9288	35.2	i198.5 i198.6 i61.4 i61.4	i115.6 i115.6	$12e_u^2 12e_u^1 12e_u^1$	2.4485	2.437

[a] E_{BP86} and E_{B3LYP} energies are in hartree. [b] Energy difference between the actual form and the lowest energy form in kcal·mol^{-1}. [c] i_{BP86} and i_{B3LYP} are the imaginary normal-mode frequencies in cm^{-1}. [d] Fe−Fe equilibrium distances in Å.

respect to the ^1C_s and $^1C_{2v}$ forms. The Fe atoms, the two μ-CO and two terminal CO groups lie in the plane orthogonal to the plane containing the four terminal CO. Jacobsen and Ziegler[7] found that the $^1D_{2h}(2)$ structure is the transition state of the $^1C_{2v} \rightarrow {}^1C_{2h}$ isomerization, using the BP86 functional. We have confirmed these results, but the same structure results in a second-order saddle point on the B3LYP PES. The first imaginary frequency (301.1i cm^{-1}) relates to the $^1C_{2v} \rightarrow {}^1C_{2h}$ isomerization, and the second imaginary frequency (200.3i cm^{-1}) points toward a structure in which the two μ-CO partially lose their bridging character. Following the eigenvector associated with the second imaginary frequency mode, we found a new stationary point of C_{2v} symmetry ($^1C_{2v}(3)$), 0.0014 hartree (0.88 kcal·mol^{-1}), which was lower in energy with respect to the $^1D_{2h}(2)$ starting point. This structure is still a second-order saddle point (290.0i and 21.4i cm^{-1}), with the first imaginary frequency mode equal to that found for the $^1D_{2h}(2)$ isomer. The fact that the second imaginary frequency is drastically lower suggests that this stationary point could be considered the genuine B3LYP transition state of the $^1C_{2v} \rightarrow {}^1C_{2h}$ isomerization. Finally, at the BP86 level this structure is not a stationary point and evolves toward the $^1D_{2h}(2)$ structure.

$^1C_{2h}$ Semibridged Isomer. This structure is a first-order saddle point. Compared with the ^1C_s isomer, the $^1C_{2h}$ is only 6.4 and 2.5 kcal·mol^{-1} higher in energy at the BP86 and B3LYP levels, respectively. The predicted Fe−Fe distance (2.587 Å for BP86, 2.628 Å for B3LYP) is longer (by 0.113 Å for BP86, 0.173 Å for B3LYP) than in the $^1C_{2v}$ form. The shorter Fe−C distance of the semibridged CO ligands is close to that of the terminal CO, and the longer Fe−C is roughly 0.2 Å longer that those of the bridged CO ligands.

The imaginary frequency mode is characterized by a collective motion of the system. At the BP86 level this frequency is very low (6.7i cm^{-1}) but becomes significantly higher at the B3LYP level (98.4i cm^{-1}). It is worth noting that the BP86 imaginary frequency value is not influenced by the computational setting of the calculation. When BP86 vibrational frequencies are computed using the finest *m*5 DFT grid-size instead of the standard *m*3,[30] the imaginary frequency becomes 10.0i cm^{-1}. Xie at al.[11] found similar results (15i and 95i cm^{-1} at the BP86 and B3LYP levels, respectively), claiming that this structure could be considered either a genuine minimum or a point very close to a minimum.

As far as the $^1C_{2v} \rightarrow {}^1C_{2h}$ isomerization is concerned, we report the BP86 and B3LYP energy diagram of the various isomers involved, considering the $^1D_{2h}(2)$ structure as transition state. Our computed barriers (see Figure 4) are in agreement with those obtained by Jacobsen et al.[7] ($^1C_{2h} \rightarrow {}^1D_{2h}$ 13.6 kcal·mol^{-1} and $^1D_{2h} \rightarrow {}^1C_{2h}$ 7.4 kcal·mol^{-1}).

$^1D_{2h}(1)$, $^1C_{2v}(2)$, and $^1C_{2h}(2)$ Unbridged Isomers. The $Fe_2(CO)_8$ singlet PES has no local minima with unbridged structure. The form with lowest energy has D_{2h} symmetry ($^1D_{2h}(1)$, Figure 1), which is a third-order saddle point. The lowest imaginary frequency mode (62.2i cm^{-1}) is associated with a displacement of the atoms toward the $^1C_{2h}$ form, and the other two imaginary modes are characterized by the mutual rotation of the $Fe(CO)_4$ group around the Fe−Fe axes, and the rotation of the $Fe(CO)_4$ fragment on the C plane. Also, in this case, Xie et al.[11] claimed that this structure might be considered a minimum for the same reason indicated above for the $^1C_{2h}$ isomer.

The $^1C_{2v}(2)$ unbridged stationary point can be considered as being formed by two $Fe(CO)_4$ fragments (Figure 1). As in the

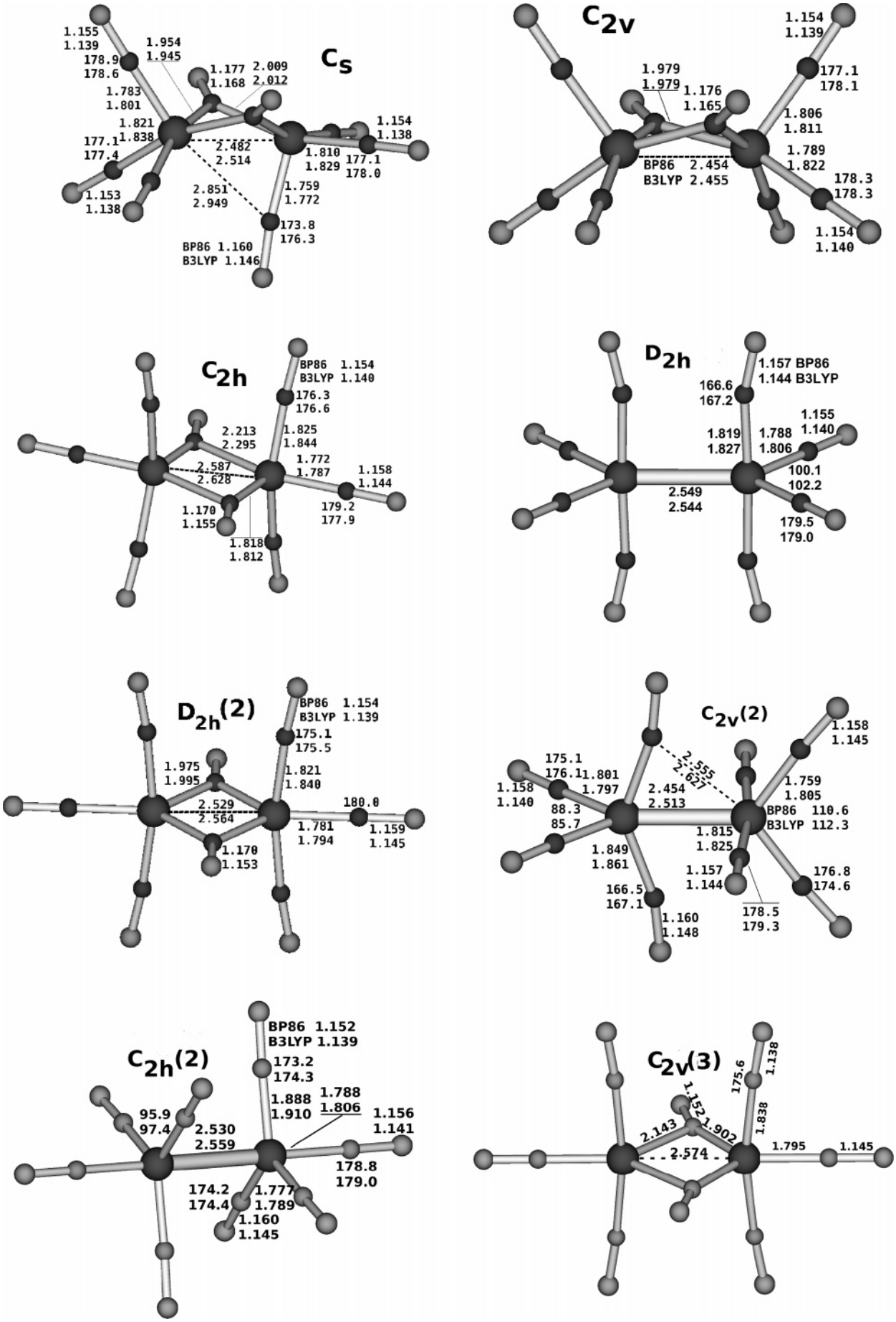

Figure 1. Singlet optimized geometry parameters. All distances and angles in Å and degree.

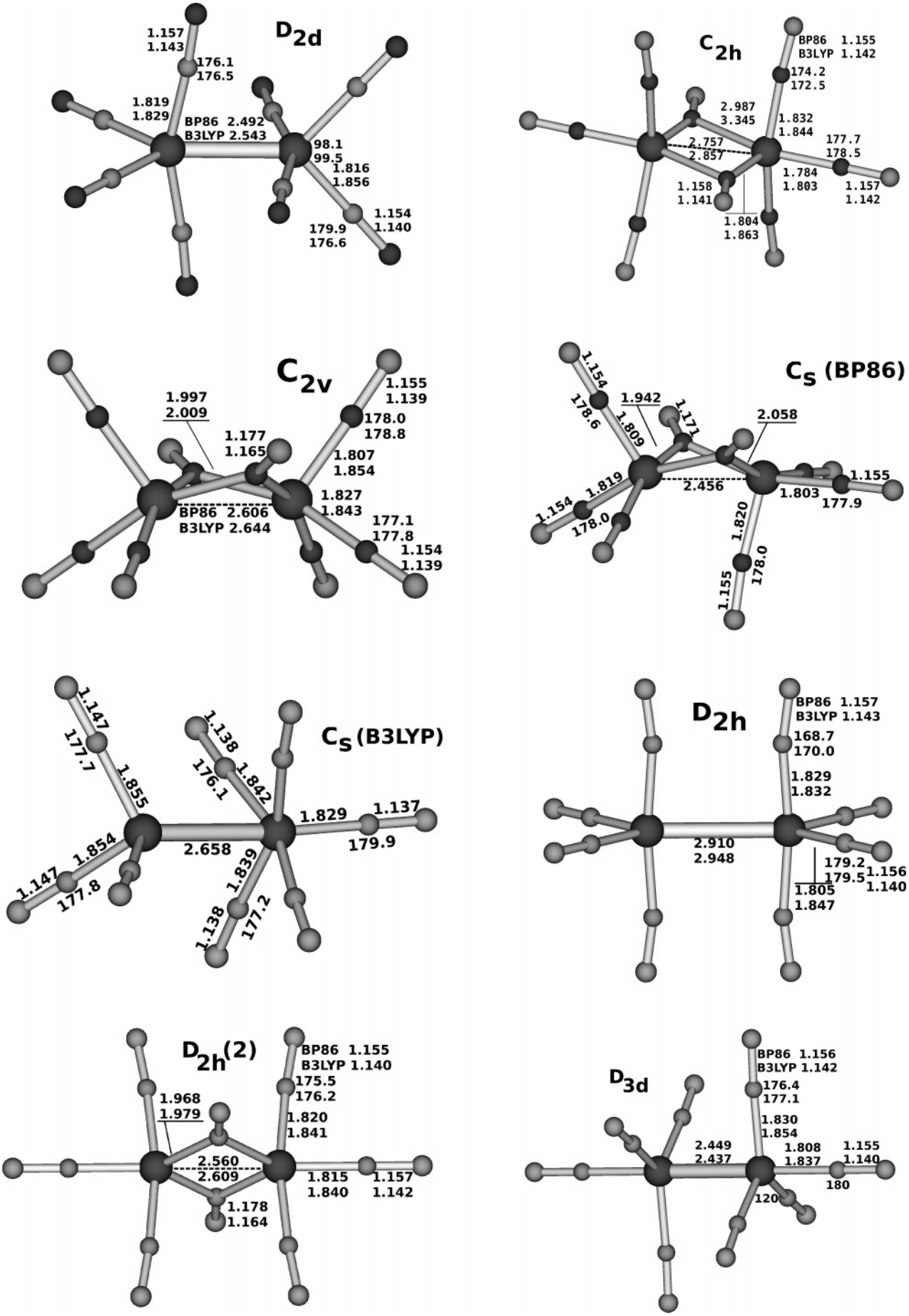

Figure 2. Triplet optimized geometry parameters. All distances and angles in Å and degree.

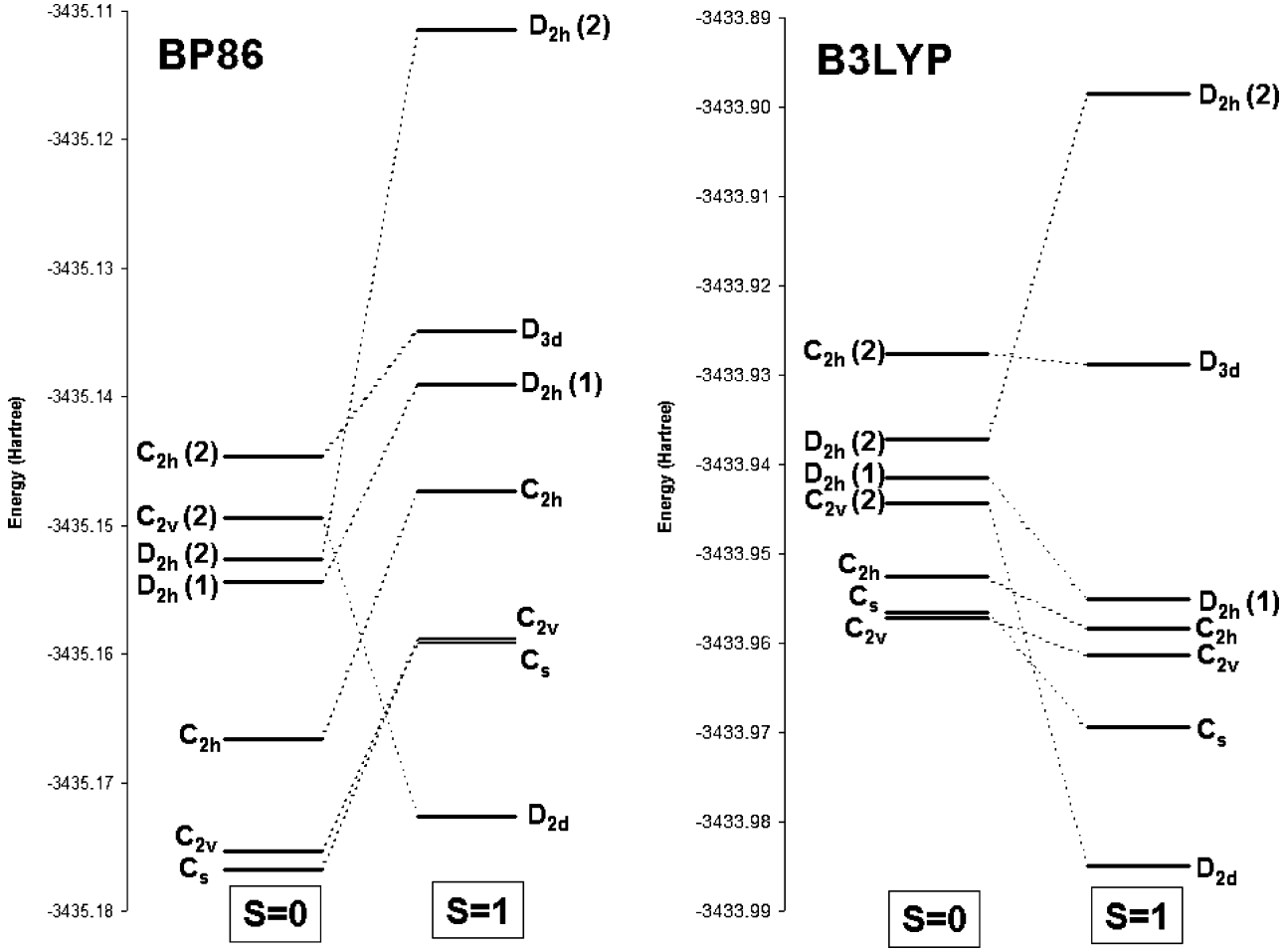

Figure 3. BP86 (left) and B3LYP (right) singlet−triplet energy diagram. Energy in hartree.

TABLE 2: Experimental and Computed CO Frequencies for Bridged $Fe_2(CO)_8$ Structures

modes	bridged exp[a]	^1C_s	BP86[b]	B3LYP	$^1C_{2v}$	BP86	B3LYP
$\nu_{CO,1}$	1814	a″	1849 (739)	1878 (1082)	b_1	1848 (771)	1884 (1142)
$\nu_{CO,2}$	1857	a′	1872 (240)	1912 (201)	a_1	1878 (152)	1940 (191)
$\nu_{CO,3}$	1867 vw	a′	1990 (297)	2076 (397)	b_2	2006 (16)	2095 (363)
$\nu_{CO,4}$	2022	a′	2015 (1012)	2104 (1178)	b_1	2020 (1388)	2104 (1606)
$\nu_{CO,5}$	2032	a″	2022 (1090)	2109 (1448)	a_1	2015 (1497)	2106 (1675)
$\nu_{CO,6}$	2055	a′	2041 (2103)	2118 (3012)	a_1	2045 (1855)	2118 (2463)

[a] Experimental frequency values from ref 4. [b] CO stretching frequencies in cm^{-1}; IR intensities in $km \cdot mol^{-1}$.

TABLE 3: Experimental $Fe_2(CO)_8$ and Computed CO Frequencies for Unbridged $Fe_2(CO)_8$ Structures

modes	unbridged exp[a]	$^1C_{2h}$	BP86[b]	B3LYP	$^1D_{2h}$	BP86	B3LYP
$\nu_{CO,1}$	1974 w	b_u	1916 (896)	2002 (1228)	b_{1u}	1983 (23)	2051 (335)
$\nu_{CO,2}$	1978 w	b_u	1997 (608)	2075 (848)	b_{2u}	1999 (2076)	2074 (2530)
$\nu_{CO,3}$	2006 s	a_u	2013 (2146)	2097 (2662)	b_{1u}	2037 (2124)	2094 (1918)
$\nu_{CO,4}$	2038 s	b_u	2029 (2176)	2101 (2471)	b_{3u}	2007 (1682)	2106 (3003)

[a] Experimental frequency values from ref 4. [b] CO stretching frequencies in cm^{-1}; IR intensities in $km \cdot mol^{-1}$.

case of $^1D_{2h}(2)$, this form results as a transition state at the BP86 level, and a second-order saddle-point at the B3LYP level. At the BP86 level this form is the highest in energy (0.0274 hartree higher in energy with respect to ^1C_s) with a Fe−Fe distance (2.454 Å) equal to that of the dibridged $^1C_{2v}$ form. At the B3LYP level this form is 0.0228 hartree higher in energy with respect to the $^1C_{2v}$ form but is slightly lower in energy (0.0072 hartree) with respect to the $^1D_{2h}(2)$ form. Following the BP86 lowest imaginary frequency mode, the structure evolves to the $^1C_{2v}$ form.

Further details of this structure are discussed in the section concerning the results for the triplet PES. The $^1C_{2v}(2)$ unbridged isomer is a third-order saddle point, very high in energy with respect to the global minimum at either the BP86 or B3LYP level, in agreement with Xie at al.[11] This form has also been identified as a local minimum for the dianion $Fe_2(CO)_8^{2-}$ by Aullon et al.[13]

3.2. Triplet PES. Seven stationary points have been characterized on the triplet PES (Table 4).

$^3D_{2d}$, $^3D_{2h}(1)$, and $^3D_{3d}$ Unbridged Isomers. The triplet PES has a global minimum of unbridged $^3D_{2d}$ symmetry. This structure can be considered as formed by two identical C_{2v}

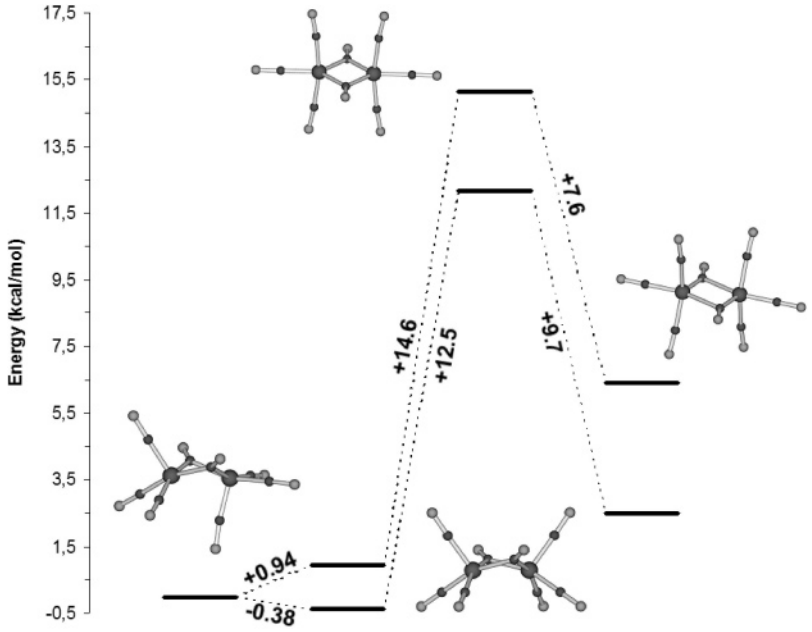

Figure 4. BP86 and B3LYP $^1C_{2v} \rightarrow {}^1C_{2h}$ isomerization path. Values of the barrier are given on kcal·mol^{-1}.

TABLE 4: Computed CO Frequencies for Unbridged Triplet State $Fe_2(CO)_8$ Structures

modes	unbridged exp[a]	$^3C_{2h}$	BP86[b]	B3LYP	$^3D_{2d}$	BP86	B3LYP
$\nu_{CO,1}$	1974 w	b_u	1980 (396)	2061 (59)	e	1980 (279)	2057 (597)
$\nu_{CO,2}$	1978 w	b_u	1996 (1087)	2084 (1616)	b_2	2002 (95)	2075 (0)
$\nu_{CO,3}$	2006 s	a_u	2005 (2144)	2089 (2633)	e	2006 (1666)	2092 (1737)
$\nu_{CO,4}$	2038 s	b_u	2027 (2013)	2103 (2631)	b_2	2029 (1480)	2116 (1831)

[a] Experimental frequency values from ref 4. [b] CO stretching frequencies in cm^{-1}; IR intensities in km·mol^{-1}.

CHART 3

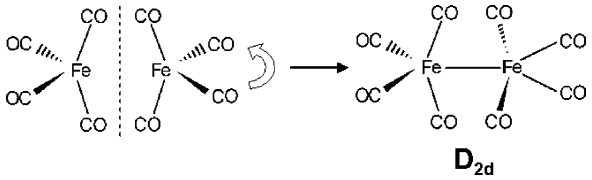

$Fe(CO)_4$ fragments in a specular position in relation to one another, and then rotated by 90° around the Fe−Fe axes (see Chart 3).

At the BP86 level, this structure is slightly higher in energy with respect to the ^1C_s singlet global minimum (2.6 kcal·mol^{-1}), and at the B3LYP level, it is lower by 17.8 kcal·mol^{-1}. This structure can be ideally obtained from the unbridged $^1C_{2v}(2)$ singlet by promoting one electron to the LUMO

$$^1Fe_2(CO)_8\ (^1C_{2v}(2)) \xrightarrow{h\nu} {}^3Fe_2(CO)_8\ (^3C_{2v}(2)) \rightarrow {}^3Fe_2(CO)_8\ (^3D_{2d})$$

In the $^1C_{2v}(2)$ singlet state, the HOMO ($20b_1$) and LUMO ($20b_2$) are very close in energy, with their major orbital contributions almost equal, but centered on different $Fe(CO)_4$ fragments. In the triplet $^3D_{2d}$ structure the two MOs become lower in energy and degenerate, forming the 20e HOMO.[32,33] For both structures the HOMO−1 is characterized by Fe−Fe bonding character (see Figure 5). The Fe−Fe distance for $^3D_{2d}$ is predicted to be 0.01 Å (BP86) or 0.026 Å (B3LYP) larger than that of the bridged ^1C_s singlet, and 0.038 Å (BP86) and 0.030 Å (B3LYP) larger than that of the unbridged $^1C_{2v}$ (2). The $^3D_{2d}$ structure has two groups of chemically different CO ligands, but the differences between Fe−C and C−O distances are very small. All Fe−C−O angles are close to 180°.

It is worth noting that the geometry parameters of the $Fe(CO)_4$ fragments of the $^3D_{2d}$ structure are close to those of the triplet $^3B_2$ $Fe(CO)_4$ ground state (see Supporting Information). We calculate the root-mean-square deviation (RMSD) according to the following definition:

$$\mathrm{RMSD}(\mathbf{u}_{Fe_2(CO)_8}, \mathbf{v}_{Fe(CO)_4}) = \left(\sum_{i=1}^{N} \frac{1}{N} \left|\left|\mathbf{u}_i - \mathbf{v}_i\right|\right|^2\right)^{1/2} \quad (2)$$

between the $Fe(CO)_4$ fragment in the triplet $^3D_{2d}$ structure (atomic position vector **u** and the singlet or triplet $Fe(CO)_4$ structures (atomic position vector **v**). At the BP86 level RMSD values are 0.123 Å for comparison with the $Fe(CO)_4$ triplet ground state, and 0.440 Å for comparison with the $Fe(CO)_4$ $^1A_1$ state.

The $^3D_{2h}(1)$ structure is a high-order transition state, very high in energy with respect to the $^3D_{2d}$ structure, with a very elongated Fe−Fe distance (2.910 Å).

The $^3D_{3d}$ structure is similar to the $^1C_{2h}(2)$ discussed for the singlet PES. This stationary point is the highest in energy on the triplet PES, and it is characterized by the shortest Fe−Fe distance and by four imaginary frequency modes. If the molecular symmetry is lowered to C_{2h}, the energy lowering is narrow (0.00069 and 0.0012 hartree at BP86 and B3LYP levels, respectively), but Fe−Fe lengthens up to 0.291 and 0.254 Å at BP86 and B3LYP levels, respectively.

$^3C_{2h}$ Semibridged Isomer. The triplet $^3C_{2h}$ form is similar to that calculated on the singlet PES. It is 0.0254 (BP86) and 0.0266 (B3LYP) hartree (15.9 and 16.7 kcal·mol^{-1}) higher in energy with respect to the $^3D_{2d}$ global minimum. The Fe−Fe distance increases by 0.264 (BP86) and 0.314 (B3LYP) Å. The two semibridged CO groups have a reduced bridging character compared with those of the singlet structure. The shorter Fe−C

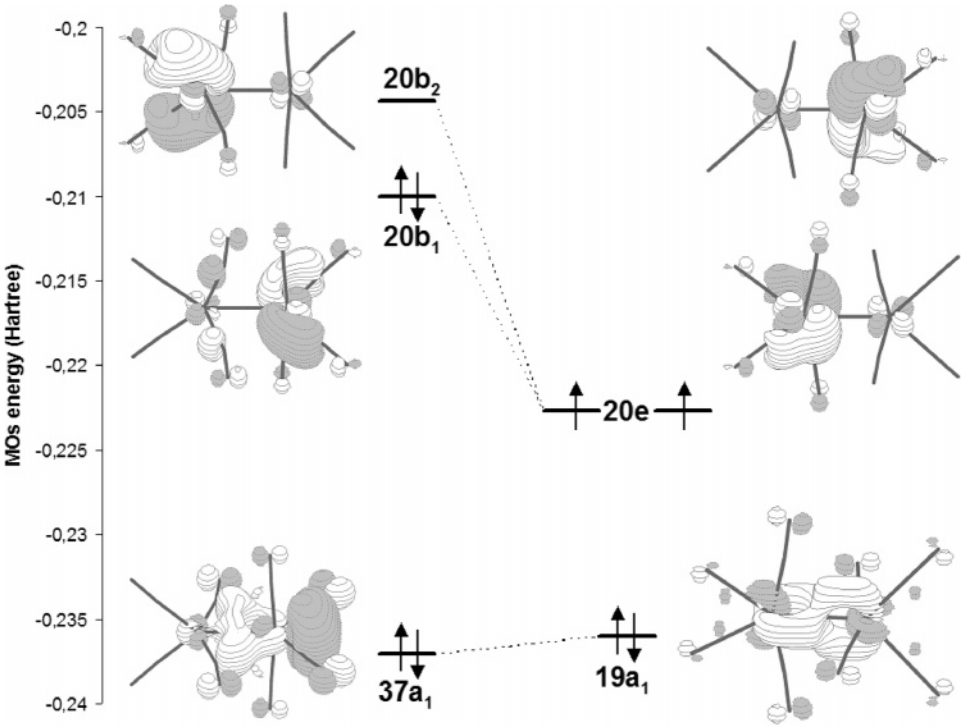

Figure 5. MO diagram for unbridged singlet $^1C_{2v}$ (left) and triplet $^3D_{2d}$ (right). Energies in hartree.

TABLE 5: Quintet−Triplet FeCO and Triplet−Singlet $Fe(CO)_4$ Adiabatic Energy Differences as a Function of the DFT Functional

FeCO	$2S+1$	E^a	$\Delta E_{\text{quintet-triplet}}{}^b$
BP86	3	−1377.2701	
	5	−1377.2587	7.2
B3LYP	3	−1376.9136	
	5	−1376.9086	3.1
PBE	3	−1376.6969	
	5	−1376.6837	8.3
PBE0	3	−1376.6740	
	5	−1376.6766	−1.6
B3LYP*	3	−1373.6933	
	5	−1373.6838	6.0
exp			3.6 ± 0.1
$Fe(CO)_4$	$2S+1$	E^a	$\Delta E_{\text{triplet-singlet}}{}^b$
BP86	1	−1717.5540	
	3	−1717.5561	−1.3
B3LYP	1	−1716.9589	
	3	−1716.9745	−9.8
PBE	1	−1716.5958	
	3	−1716.5970	−0.4
PBE0	1	−1716.4957	
	3	−1716.5140	−11.5
B3LYP*	1	−1717.3138	
	3	−1717.3203	−1.0

[a] Energies in hartree. [b] Energies in kcal·mol^{-1}.

distance is reduced by 0.014 (BP86) and 0.009 (B3LYP) Å, and the longer distance is increased by 0.774 (BP86) and 1.05 (B3LYP) Å. This effect can be rationalized by considering that in the triplet state the doubly occupied HOMO of the singlet $^1C_{2h}$ state becomes singly occupied. This MO has a marked bonding character for the longer Fe−C_μ bond, and therefore, the depletion of electron density in that region will lead to lengthening of the bond.[31] This stationary point has one normal mode with low imaginary frequency (5.9i and 27.1i cm^{-1} at the BP86 and B3LYP levels, respectively).

TABLE 6: Singlet−Triplet Adiabatic Energy Differences as a Function of the DFT Functional

	$^1C_s{}^a$	$^1C_{2v}{}^a$	$^3D_{2d}{}^a$	$\Delta E_{\text{triplet-singlet}}{}^b$
BP86	−3435.1768	−3435.1754	−3435.1727	2.6
B3LYP	−3433.9565	−3433.9571	−3433.9849	−17.4
PBE	−3433.2687	−3433.2668	−3433.2622	4.1
PBE0	−3433.0515	−3433.0522	−3433.0770	−16.0
B3LYP*	−3423.8693	−3423.8700	−3433.8917	−13.6

[a] Energies in hartree. [b] Energies in kcal·mol^{-1}.

TABLE 7: Singlet−Triplet Adiabatic Energy Differences as a Function of the Basis Set Quality

DFT	basis	$^1C_s{}^a$	$^1C_{2v}{}^a$	$^3D_{2d}{}^a$	$\Delta E_{\text{triplet-singlet}}{}^b$
BP86	TZVP	−3435.1768	−3435.1754	−3435.1727	2.6
	TZVPP	−3434.2264	−3435.2256	−3435.2235	1.8
	QZVP	−3435.3366	−3435.3363	−3435.3333	2.1
B3LYP	TZVP	−3433.9565	−3433.9571	−3433.9849	−17.4
	TZVPP	−3434.0105	−3434.0116	−3434.0403	−18.0
	QZVP	−3434.1176	−3434.1191	−3434.1471	−17.7

[a] Energies in hartree. [b] Energies in kcal·mol^{-1}.

$^3C_{2v}$, ^3C_s, and $^3D_{2d}$(2) Bridged Isomers. The $^3C_{2v}$ dibridged structure is a first-order saddle point on the triplet PES. Fe−Fe distance is increased by 0.152 and 0.189 Å with respect to the corresponding singlet state at the BP86 and B3LYP levels. The remaining bond distances and bond angles do not change significantly. The BP86 triplet ^3C_s dibridged structure has a Fe−Fe distance slightly shorter than in the singlet state. Using the B3LYP functional, the geometry optimization of the ^3C_s dibridged structure leads to the $Fe(CO)_3$−$Fe(CO)_5$ unbridged structure shown in Figure 2. The $Fe(CO)_5$ fragment has local C_{4v} symmetry, whereas in the $Fe(CO)_3$ fragment the CO ligand lies in the σ plane. The Fe−Fe distance is increased with respect to either the singlet B3LYP C_s or the triplet BP86 C_s structure. All C_{2v} and C_s triplet structures are first-order saddle points. Except in the case of the B3LYP ^3C_s form, the imaginary frequency mode is characterized by atom displacements toward the $^3D_{2d}$ structure.

TABLE 8: Single-Point Coupled-Cluster Single and Double $Fe_2(CO)_8$ Singlet−Triplet Adiabatic Energy Differences

geometry	level	^1C_s[b]	$^1C_{2v}$	$^1D_{2d}$	$\Delta E_{D_{2d}/C_{2v}}$[c]
BP86	UHF/RHF	−3426.5480	−3426.5476	−3426.6984	−94.6
	CCSD(55,70)[a]	−3427.8155	−3427.8255	−3427.8447	−12.1
B3LYP	UHF/RHF	−3426.5778	−3426.5780	−3426.7380	−100.4
	CCSD(55,70)[a]	−3427.8169	−3427.8308	−3427.8516	−13.1
	CCSD(55,118)[a]		−3428.6489	−3428.6760	−17.0

[a] CCSD(n,m) where n and m refer to the numer of occupied and virtual MOs included in the CC computations. [b] Energies in hartree. [c] Energies in kcal·mol^{-1}.

Finally, the bridged $^3D_{2h}(2)$ structure is a high-order saddle point, and it represents the state that is highest in energy among all the isomers under consideration.

4. Discussion

4.1. CO Dissociation Path on the $Fe_2(CO)_9$ Triplet PES. One important consequence of the $Fe_2(CO)_8$ triplet PES exploration is the possibility of fully characterizing the path for the dissociation of a carbonyl group of $Fe_2(CO)_9$ on the first triplet PES. In a previous work[12] it was found that the 1^3B_2 $Fe_2(CO)_9$ state is not bound with respect to the dissociation $Fe_2(CO)_8$ (C_{2v}) + CO. In this work we found that the triplet $^3C_{2v}$ $Fe_2(CO)_8$ structure is a transition state. If one proceeds in the direction of the imaginary frequency mode, the structure evolves to the $^3D_{2d}$ form. Therefore, the complete reaction path of the triplet state is the following

$$^1Fe_2(CO)_9\ (^1D_{3h}) \xrightarrow{h\nu} {}^3Fe_2(CO)_8\ (^3C_{2v}) + CO \rightarrow {}^3Fe_2(CO_8)\ (^3D_{2d}) + CO$$

4.2. Vibrational Frequencies. The computed CO stretching frequencies of bridged and unbridged forms were compared with the experimental values of Poliakoff et al.[3] The differences among BP86 and B3LYP values are often considerable but are reduced when B3LYP values are scaled using the usual 0.9614 factor. For this reason we have limited the discussion to the BP86 values only.

For the bridged forms, the ^1C_s frequencies are slightly closer to the experimental values than those of $^1C_{2v}$, according to the sum of the absolute errors $\sum_i(|\nu_{exp,i} - \nu_{calc,i}|)$ (204 cm^{-1} for ^1C_s and 223 cm^{-1} for $^1C_{2v}$). Jacobsen et al.[7] reached similar conclusions. The case of the unbridged form is more controversial: the $^1D_{2h}$ form is ruled out because of its absorption intensity pattern, which differs considerably from that of the experiment, in agreement with Jacobsen et al.[7] But either $^1C_{2h}$ or unbridged $^1C_{2v}$ patterns are compatible with the experimental one, and this latter aspect was not taken into account by Jacobsen. The error for $^1C_{2h}$ is 93 cm^{-1} and becomes 53 cm^{-1} for unbridged $^1C_{2v}$. The error becomes even smaller if we consider the $^1D_{2d}$ values (40 cm^{-1}).

4.3. On the Adiabatic Energy Difference between Triplet Unbridged and Singlet Bridged $Fe_2(CO)_8$ Structures. ***4.3.1. The DFT Level.*** In the results section, we have seen that the BP86 and B3LYP pictures for $Fe_2(CO)_8$ singlet and triplet PES are different: the bridged ^1C_s structure is the ground state when the BP86 fuctional is used, whereas the unbridged $^3D_{2d}$ is the ground state when the B3LYP functional is used. This result prompted us to further investigate these structures. Therefore we have considered three additional DFT functionals, the GGA PBE,[41,42] the hybrid PBE0,[43] and the B3LYP*.[44] The last is a modified version of B3LYP in which the c_3 parameter of the Hartree−Fock exact exchange is set equal to 0.15 instead of to 0.20. This functional has been proved to be more reliable in the computation of energy splitting between high-spin and low-spin in iron complexes.[45] As a preliminary benchmark, we computed the adiabatic energy differences for FeCO and $Fe(CO)_4$ using the suite of DFT functionals listed above. In fact, it is known that these two systems have high-spin ground state. The results are reported in Table 5.

FeCO (iron monocarbonyl) has a triplet ground state. The quintet state is 3.6 ± 0.1 kcal·mol^{-1} higher in energy compared to the triplet, as determined by photoelectron spectra.[39] Gas-phase experiments established a linear ground state geometry, with Fe−C and C−O bond lengths equal to 1.727 and 1.159 Å, respectively. All theoretical quintet−triplet energy gap values show that the triplet state is more stable than the quintet state, in agreement with the experimental evidence. These results are in agreement with those obtained by Adamo et al. (5.5 kcal·mol^{-1}, B3LYP/DZ),[40] and Wang et al. (5.9 kcal·mol^{-1} BP86, 2.6 kcal·mol^{-1} B3LYP).[37]

The $^1A_1$ singlet and $^3B_2$ triplet $Fe(CO)_4$ states have C_{2v} symmetry, with the latter lower in energy than to the former. The structure and the energetics of $Fe(CO)_4$ states are consolidated facts, but the previous theoretical values of the singlet−triplet energy gaps are spread between 0.5 and 20 kcal·mol^{-1}.[36] The predicted DFT singlet−triplet gaps are 0.7, 9.4, and 0.5 kcal·mol^{-1} (triple-ζ BPW91, B3PW91, and BP86, respectively[34]), and 0.5 and 8.7 kcal·mol^{-1} (BLYP and B3LYP respectively, with 6-31G(p,d) on C and O and Hay−Wadt pseudopotential on Fe with the double-ζ basis set[37]). Energy gap values were also obtained using single-point energy coupled-cluster calculations. A first value of 8.8 kcal·mol^{-1} [34] was obtained using triple-ζ basis sets and B3PW91 optimized geometries and is coherent with Barnes et al.'s[35] value of 15 ± 5 kcal·mol^{-1} obtained with modified coupled-pair functional calculations; a second value of 2.33 kcal·mol^{-1} was recently obtained by Carreon et al.[38] on B3LYP optimized geometries, using CCSD(T) with a large basis set (cc-pVQZ on Fe, cc-pVTZ on CO). This last value can be considered as the most accurate obtained up to this point.

The results in Table 5 show that the adiabatic energy differences computed with the five DFT functionals under consideration are in qualitative agreement with one another, except for the case of PBE0 for FeCO. The best agreement for FeCO is obtained with B3LYP functional. In the case of $Fe(CO)_4$, the best agreement between the DFT value and high-level CCSD(T)[38] is found with B3LYP*. These results are in agreement with Lawson Daku et al.[27] findings on the iron(II) tris(2,2′-bispyridine) complex. Furthermore, at variance with Fouquenau et al. finding[25] on iron(II) complexes with low-field ligands (H_2O and NH_3), PBE0 gives the worst agreement on adiabatic energy differences, because it overstabilizes high-spin states. In this particular case, the fact that CO is a high-field ligand involved in unsaturated low-valence iron complexes could play an important role.

The trend is clear: GGA functionals stabilize the low-spin state, and hybrid functionals stabilize the high-spin state. When the contribution of the exact Hartree−Fock exchange is lowered (B3LYP*), the high-spin state is stabilized to a lesser extent.

The optimized geometry parameters do not differ significantly (see Supporting Information). It is worth noting that triplet FeCO is a linear molecule, and the quintet state is slightly bent (see Supporting Information). This fact was not taken into account by Barnes et al.,[35] because they constrained the Fe−C−O angle to 180°.

We will now consider $Fe_2(CO)_8$. All the computed adiabatic energy differences are listed in Table 6. As previously discussed, the GGA functionals predict the triplet state as beign more stable than the singlet state, whereas the opposite is true when hybrid functionals, including B3LYP*, are considered. It is definitely clear that DFT does not provide a clear-cut answer regarding the relative stability of singlet and triplet $Fe_2(CO)_8$. The effect of the exact Hartree−Fock exchange is crucial: we have computed the energy gap as a function of the c_3 coefficient of the exact HF exchange within the definition of the B3LYP* functionals, and we have verified a linear trend (see Supporting Information), as previously shown by Reiher et al.[44] for other high-spin−low-spin energy gaps in iron complexes.

Finally, we considered the effect of the basis set quality on the adiabatic energy differences computed at BP86 and B3LYP level of theory (see Table 7). Starting from the TZVP results, we also employed TZVP plus one f function for each atom (hereafter TZVPP[47]) and quadruple-ζ (hereafter QZVP[48]) basis sets. The optimized geometries using higher quality basis sets do not differ significantly from those obtained with the TZVP basis set with either B3LYP or BP86 functionals. The effect of the improved basis sets on the adiabatic energy differences does not exceed 1.0 kcal·mol^{-1} and evolves in the direction of the triplet state stabilization.

4.3.2. Single-Point Energy Computations at the CCSD Level. In the above section, we have concluded that the DFT level of theory is not able to give an unequivocal answer concerning the spin multiplicity of the $Fe_2(CO)_8$ ground state. Therefore computations at correlated ab initio levels become essential to gain further information. We decided to carry out CCSD single-point energy computations using the TZVP basis set. All valence electrons (except 1s of C and O, 1s, 2s, 2p of Fe) were correlated. In a first set of calculations we included 70 virtual MOs (CCSD(55,70)).[49] CCSD energies (see Table 8) computed on the B3LYP/TZVP optimized geometries are always lower than those computed using the corresponding BP86/TZVP geometry (0.0014, 0.0111, and 0.0083 hartree for ^1C_s, $^1C_{2v}$, and $^1D_{2d}$ forms respectively). Furthemore, the singlet $^1C_{2v}$ form is lower in energy compared to ^1C_s form by 8.4 kcal·mol^{-1}. The triplet state is stabilized by 13.1 kcal·mol^{-1} compared to the singlet state. Finally, we included a further 48 virtual MOs in the CCSD computations (CCSD(55,118)). The resulting $\Delta E_{\text{singlet-triplet}}$ increased by 4.9 kcal·mol^{-1}. Although the quality of these computations can be improved, CCSD results are in agreement with the DFT/B3LYP picture given above.

5. Conclusions

In this paper we explored the PES of the singlet and triplet states of the binuclear $Fe_2(CO)_8$ complex. The results of the topology of the singlet PES have essentially confirmed the results of previous theoretical works. The differences between the results produced by BP86 and B3LYP functionals do not change the global picture of the $Fe_2(CO)_8$ singlet state. The exploration of the triplet PES has never been carried out previously, and some unexpected results were obtained. The global triplet minima is the unbridged $^3D_{2d}$ structure. The adiabatic energy difference between singlet and triplet lowest energy isomers computed with five different DFT functionals reveals that hybrid functionals stabilize the high-spin state, and GGA functionals stabilize the low-spin state. The role of the exact Hartree−Fock exchange is crucial: by reducing its contribution using modified B3LYP* functionals, the triplet remains lower in energy with respect to the singlet, even if to a lesser extent. We conclude that the DFT level of theory is not able to establish the actual $Fe_2(CO)_8$ ground state. Nevertheless, DFT/B3LYP results are further corroborated by single-point energy CCSD computations on B3LYP and BP86 optimized geometries: in both cases CCSD favors $^3D_{2d}$.

Fletcher et al.[4] claimed that the first product of $Fe_2(CO)_9$ photolysis is the bridged isomer $Fe_2(CO)_8$. This experimental evidence is supported by the accurate analysis of the IR spectra of the $Fe_2(CO)_9$ photoproducts, and it is corroborated by the comparison of this data with our computed CO stretching frequencies for bridged $Fe_2(CO)_8$ forms. In addition, CO computed vibrational frequencies indicate that the triplet $^1D_{2v}$ $Fe_2(CO)_8$ structure is compatible with the corresponding experimental values for the unbridged form.

The conclusion of the paper by Poliakoff and Turner[36] on $Fe(CO)_4$ holds also in this case. Our study placed in evidence the need for further investigations on $Fe_2(CO)_8$. The crucial step is the accurate determination of the bridged and unbridged structures. This might be possible through an ultrafast electron diffraction (UED) experiment, as was performed in the case of $Fe(CO)_4$.[46] Such experiments would also provide important experimental information about the photochemical pathway of the $Fe_2(CO)_9$ CO photolysis. Finally, it would be extremely important to measure the adiabatic energy difference $\Delta E_{\text{triplet-singlet}}$ between singlet and triplet $Fe_2(CO)_8$, or at least to determine its sign. This information could be also obtained from the UED experiment. From the computational point of view, it would be important to compute the $\Delta E_{\text{triplet-singlet}}$ at highly correlated levels of theory, as already performed for $Fe(CO)_4$.[38]

Supporting Information Available: FeCO and $Fe(CO)_4$ optimized geometries, plot of B3LYP* $Fe_2(CO)_8$ singlet−triplet energy gap versus parameter. This material is available free of charge via the Internet at http://pubs.acs.org.

References and Notes

(1) Hoffmann, R. *Angew. Chem., Int. Ed. Engl.* **1982**, *21*, 711.
(2) Peters, W. J.; Lanzillotta, W. N.; Lemon, B. J.; Seefeld, L. C. *Science* **1998**, *282*, 1853.
(3) Poliakoff, M.; Turner, J. J. *J. Chem. Soc. A* **1971**, 1403.
(4) Fletcher, S. C.; Poliakoff, M.; Turner, J. J. *Inorg. Chem.* **1986**, *25*, 3597.
(5) Fedrigo; Haslett; Moskovits. *J. Am. Chem. Soc.* **1996**, *118*, 5083.
(6) Markin, E. M.; Sugawara, K. *J. Phys. Chem. A* **2000**, *104*, 1416.
(7) Jacobsen, H.; Ziegler, T. *J. Am. Chem. Soc.* **1996**, *118*, 4631.
(8) Barckholtz, T. A.; Bursten, B. E. *J. Organomet. Chem.* **2000**, *596*, 212.
(9) Baev, A. K. *Russ. J. Chem.* **1980**, *54*, 1.
(10) Jang, J. H.; Lee, J. G.; Lee, H.; Xie, Y.; Schaefer, F. *J. Phys. Chem. A* **1998**, *102*, 5298.
(11) Xie, Y.; Schaefer, F.; King, R. B. *J. Am. Chem. Soc.* **2000**, *122*, 8746.
(12) Bertini, L.; Greco, C.; De Gioia, L.; Fantucci, P. *J. Phys. Chem. A* **2006**, *110*, 12900.
(13) Aullon, G.; Alvarez, S. *Organometallics* **2001**, *20*, 818.
(14) Moore, D. T.; Oomens, J.; Eyler, J. R.; Meijer, G.; Helden, G.; Ridge, D. p. *J. Am. Chem. Soc.* **2004**, *126*, 14726.
(15) Becke, A. D. *Phys. Rev. A* **1988**, *38*,3098.
(16) Perdew, J. P. *Phys. Rev. B* **1986**, *33*,8822.
(17) Lee, C.; Yang, W.; Parr, R. G. *Phys. Rev. B* **1988**, *37*,785.
(18) Vosko, S.; Wilk, L.; Nussair, M. *Can. J. Phys.* **1980**, *58*,1200.
(19) Schaefer, A.; Huber, C.; Ahlrichs, R. *J. Chem. Phys.* **1994**, *100*, 5829.
(20) Ahlrichs, R.; Bar, M.; Haser, M.; Horn, H.; Kolmel, C. *Chem. Phys. Lett.* **1989**, *62*, 165.

(21) Eichkorn, K.; Weigend, F.; Treutler, O.; Ahlrichs, R. *Theor. Chem. Acc.* **1997**, *97*, 119.

(22) Barckholtz, T. A.; Bursten, B. E. *J. Organomet. Chem.* **2000**, *596*, 212.

(23) Frisch, M. J.; Trucks, G. W.; Schlegel, H. B.; Scuseria, G. E.; Robb, M. A.; Cheeseman, J. R.; Montgomery, J. A., Jr; Vreven, T.; Kudin, K. N.; Burant, J. C.; Millam, J. M.; Iyengar, S. S.; Tomasi, J.; Barone, V.; Mennucci, B.; Cossi, M.; Scalmani, G.; Rega, N.; Petersson, G. A.; Nakatsuji, H.; Hada, M.; Ehara, M.; Toyota, K.; Fukuda, R.; Hasegawa, J.; Ishida, M.; Nakajima, T.; Honda, Y.; Kitao, O.; Nakai, H.; Klene, M.; Li, X.; Knox, J. E.; Hratchian, H. P.; Cross, J. B.; Bakken, V.; Adamo, C.; Jaramillo, J.; Gomperts, R.; Stratmann, R. E.; Yazyev, O.; Austin, A. J.; Cammi, R.; Pomelli, C.; Ochterski, J. W.; Ayala, P. Y.; Morokuma, K.; Voth, G. A.; Salvador, P.; Dannenberg, J. J.; Zakrzewski, V. G.; Dapprich, S.; Daniels, A. D.; Strain, M. C.; Farkas, O.; Malick, D. K.; Rabuck, A. D.; Raghavachari, K.; Foresman, J. B.; Ortiz, J. V.; Cui, Q.; Baboul, A. G.; Clifford, S.; Cioslowski, J.; Stefanov, B. B.; Liu, G.; Liashenko, A.; Piskorz, P.; Komaromi, I.; Martin, R. L.; Fox, D. J.; Keith, T.; Al-Laham, M. A.; Peng, C. Y.; Nanayakkara, A.; Challacombe, M.; Gill, P. M. W.; Johnson, B.; Chen, W.; Wong, M. W.; Gonzalez, C. and Pople, J. A. *Gaussian 03*, revision C.02; Gaussian, Inc.: Wallingford, CT, 2004.

(24) Fouqueau, A.; Mer, S.; Casida, M. E.; Daku, L. M. L.; Hauser, A.; Mineva, T.; Neese, F. *J. Chem. Phys.* **2004**, *120*, 9473.

(25) Fouqueau, A.; Mer, S.; Casida, M. E.; Daku, L. M. L.; Hauser, A.; Neese, F. *J. Chem. Phys.* **2005**, *122*, 044110.

(26) Zein, S.; Borshch, S. A.; Fleurat-Lessard, P.; Casida, M.; Charmette, H. *J. Chem. Phys.* **2007**, *126*, 014105.

(27) Lawson Daku, L. Max.; Vargas, A.; Hauser, A.; Fouqueau, A.; Casida, M. *Chem. Phys. Chem.* **2005**, *6*, 1393.

(28) Bruschi, M.; Fantucci, P.; De Gioia, L. *Inorg. Chem.* **2004**, *43*, 3733.

(29) Nicolet, Y.; de Lacey, A. L.; Vernede, X.; Fernandez, V. M.; Hatchikian, E. C.; Fontecilla-Camps, J. C. *J. Am. Chem. Soc.* **2001**, *123*, 1596.

(30) The gridsize for the exchange-correlation term quadrature are of 78 520 and 256 650 points for *m*3 and *m*5, respectively.

(31) We performed a preliminary search at the bond critical points (BCP) for the singlet and triplet C_{2h} structures according the quantum theory of atom in molecules (Contez-Guzman, F.; Bader, R. F. W. *Coord. Chem. Rev.* **2005**, *249*, 633) using the AIMPAC code (Beigler-Konig, F, W.; Bader R. W. F.; Tang, H.-T. *J. Comput. Chen.* **1982**, *317*, 3). For the singlet state, we found that each carbon atom that belongs to the semibridged CO groups forms two Fe−C BCP which are slightly closer to the carbon atom. For the shorter Fe−C distance, the electron density at the BCP is $\rho(\mathbf{r}_{BCP}) = 0.145$ au, for the longer $\rho(\mathbf{r}_{BCP}) = 0.0630$ au. The Fe−Fe BCP is also found with $\rho(\mathbf{r}_{BCP}) = 0.0441$ au. For the triplet state, the BCP along the longer distance Fe−C disappears, and the BCP for the shorter Fe−C bond has features similar to that of singlet state ($\rho(\mathbf{r}_{BCP}) = 0.143$ au). The Fe−Fe BCP is also found, but with lower electron density ($\rho(\mathbf{r}_{BCP}) = 0.0260$ au).

(32) The D_{2d} E symmetry species is transformed under the C_{2v} point group as $B_1 + B_2$.

(33) Full, J.; Gonzalez, L.; Daniel, C. *J. Phys. Chem. A* **2001**, *105*, 184.

(34) Gonzalez-Blanco, O.; Branchadella, V. *J. Chem. Phys.* **1999**, *110*, 778.

(35) Barnes, L. A.; Rosi, M.; Bauschtlicher, C. W., Jr. *J. Chem. Phys.* **1991**, *94*, 2031.

(36) Poliakoff, M.; Turner, J. J. *Angew. Chem., Int. Ed.* **2001**, *40*, 2809.

(37) Wang, W.; Weitz, E. *J. Phys. Chem. A* **1997**, *101*, 2358.

(38) Carreon-Macedo, J. L.; Harvey, J. N. *Phys. Chem. Chem. Phys.* **2006**, *8*, 93.

(39) Villalta, P. W.; Leopold, D. G. *J. Chem. Phys.* **1993**, *98*, 7730.

(40) Adamo, C.; Lelj, F. *J. Chem. Phys.* **1995**, *103*, 10605.

(41) Perdew, J. P.; Burke, K.; Ernzerhof, M. *Phys. Rev. Lett.* **1996**, *77*, 3865.

(42) Perdew, J. P.; Burke, K.; Ernzerhof, M. *Phys. Rev. Lett.* **1997**, *78*, 1396.

(43) Adamo, C.; Scuseria, G.; Barone, V. *J. Chem Phys.* **1999**, *111*, 2889.

(44) Reiher, M.; Salomon, O.; Hess, B. A. *Theo. Chem. Acc.* **2001**, *107*, 48.

(45) Salomon, O.; Reiher, M.; Hess, B. A. *J. Chem. Phys.* **2002**, *117*, 4729.

(46) Ihee, H. H.; Cao, J.; Zewail A. H. *Angew. Chem., Int. Ed.* **2001**, *40*, 1532.

(47) Schaefer, A.; Horn, H.; Ahlrichs, R. *J. Chem. Phys.* **1992**, *97*, 2571.

(48) Weigend, F.; Furche, F.; Ahlrichs, R. *J. Chem. Phys.* **2003**, *119*, 12753.

(49) $Fe_2(CO)_8$ has 164 electrons; the TZVP basis set generates 82 occupied and 288 virtual MOs at restricted level; 55 of the 82 occupied MOs are valence occupied MOs.